Elastic behaviour and radiation tolerance in Nb-based 211 MAX phases

Hadi, M. A., Christopoulos, S., Chroneos, A., Naqib, S. H. & Islam, A. K. M. A.

Original citation & hyperlink:
Hadi, MA, Christopoulos, S, Chroneos, A, Naqib, SH & Islam, AKMA 2020, 'Elastic behaviour and radiation tolerance in Nb-based 211 MAX phases', Materials Today Communications, vol. 25, 101499.
https://dx.doi.org/10.1016/j.mtcomm.2020.101499

DOI 10.1016/j.mtcomm.2020.101499
ESSN 2352-4928

Publisher: Elsevier

Elastic behaviour and radiation tolerance in Nb-based 211 MAX phases

M.A. Hadi[1*], S.-R.G. Christopoulos[2], A. Chroneos[2,3†], S.H. Naqib[1], and A.K.M.A. Islam[1,4]

[1]Department of Physics, University of Rajshahi, Rajshahi 6205, Bangladesh
[2]Faculty of Engineering and Computing, Coventry University, Priory Street, Coventry CV1 5FB, UK
[3]Department of Materials, Imperial College London, London SW7 2BP, UK
[4]International Islamic University Chittagong, Kumira, Chittagong 4318, Bangladesh

Abstract

MAX phase carbides are a set of materials that have attracted the research and industrial interest due to their unique combination of metallic and ceramic properties. In recent experimental studies it was determined that Nb-based MAX phases have good mechanical and thermal properties. In the present systematic density functional theory study we examine the elastic behaviour and radiation tolerance of a range of Nb_2AC (A = Al, Ga, Ge, In, Sn, As, P, and S) MAX phases. It is found that the Nb-based 211 MAX phases studied here are mechanically stable and elastically anisotropic. Elastically, Nb_2GeC possesses the highest level of anisotropy and Nb_2InC, the lowest. The cross-slip pinning process is enhanced in Nb_2GeC that is considerably reduced in Nb_2InC. Nb_2GeC, Nb_2SnC, and Nb_2SC are ductile, whereas the other Nb-based MAX phases considered here are brittle in nature. In particular, Nb_2GeC is highly ductile and Nb_2AlC is more brittle. Nb_2PC and Nb_2SnC are respectively, more stiff and flexible under tension or compression. Nb_2SnC has the best thermal shock resistance among the Nb-based MAX phase carbides studied here. Regarding the radiation tolerance of these MAX phases it is anticipated that Nb_2SnC will be the most resistant to radiation.

Keywords: MAX phases; First-principles calculations; Elastic properties; Defect processes

1. Introduction

A large number of ternary compounds mainly carbides, some nitrides and a boride in hexagonal crystal system belong to the materials family known as "MAX phases" [1,2]. MAX phases are characterized with both metallic and ceramic properties. Chemically, they are defined as $M_{n+1}AX_n$, where M is an early transition metal, A is A-group element and X is carbon, nitrogen or boron and *n* is an integer commonly from 1–3 but with a highest value of 6 [3]. Depending on *n*, MAX phases are classified as 211, 312, and 413 phases for *n* = 1, 2, and 3, respectively. In essence, the MAX phases consist of $M_{n+1}X_n$ ceramic layers inserted between the metallic A-layers of one-atom-thick (i.e. MAX phases are termed as nanolaminates). The layered structure of MAX phases is the key for their metallic and ceramic properties including damage tolerance, thermal and electrical conductivities, thermal shock resistance and machinability, commonly demonstrated by metals, together with light weight, high stiffness, resistance to oxidation and corrosion resistance that are characteristics of ceramics [4,5]. Furthermore, MAX phases are reported to show a good capability to annihilate radiation-induced defects at high temperatures [6–8]. MAX phase compounds are now being considered as promising candidate materials for application in accident tolerant fuel (ATF) claddings in 3rd generation (Gen-III) light-water reactors (LWRs) and future (Gen-IV) fission plants [9–11]. MAX phases, with Zr, Nb and/or Ti as an M element have recently been fabricated as potential fuel cladding coating materials either for ATF applications (LWRs), or for next-generation nuclear systems with corrosive primary coolants (e.g. Gen-IV lead- cooled fast reactors, LFRs) [12–18].

To date, about 80 MAX phases are synthesized with the majority being 211 phases, which comprise 58 members [19]. So far, different 11 transition metals are found to occupy the M-site in MAX phases. Nb has nine carbide phases in the 211 MAX family, namely Nb_2AlC, Nb_2PC, Nb_2SC, Nb_2CuC, Nb_2GaC, Nb_2GeC, Nb_2AsC, Nb_2InC, and Nb_2SnC. Among those, Nb_2SC, Nb_2AsC, Nb_2InC and Nb_2SnC are superconductors [19]. Nb_2AlC has attracted considerable interest as it possesses good mechanical and thermal properties, constituting it a promising material for high-temperature structural and functional applications [20–22]. Nb_2PC, typically of phosphorus containing MAX phases, has larger elastic

*Corresponding author: hadipab@gmail.com
†Corresponding author: ab8104@coventry.ac.uk

constants compared to most other related MAX phases [23]. Nb_2GaC and Nb_2InC are promising candidates for successful exfoliation into 2D MXene [24] systems. Nb_2SnC is the first phase reported with an excellent electrochemical performance in Li-ion electrolyte. The Li-ions interact with Sn to form Li_xSn, which can progressively exfoliate some layers and single layers or Nb_2C, remove Sn from the structure, and break the large MAX phase materials into minor and more electrochemically active units, assisting pseudocapacitive reaction and contributing to capacity improvement. Nb_2SnC is highly conductive as it significantly increases its electrochemical performance. As anode in batteries it combines the advantages of layered materials and alloying elements and has a longer life cycle than most of the other Sn-containing nanomaterials [25,26]. Nb_2SC is a better dielectric material [27]. Nb_2CuC is an exceptional MAX phase whose A-site is also occupied by a transition metal Cu instead of A-group element [28]. Nb_2AsC has the lowest superconducting transition temperature amongst all MAX phase superconductors [19].

Therefore, Nb-containing 211 MAX phase carbides have significant diversity in their properties. Understanding the elastic behaviour of materials is essential to decide on where they are most suitable, whereas the defect processes in crystals provides the information regarding the radiation tolerance of materials. The elastic properties of these compounds have been studied individually in previous studies with different methodologies and codes [19,27,29–37]. The defect processes in these crystals have never been investigated. In this study, we aim to investigate the elastic behaviour and defect processes in the Nb-based 211 MAX phase carbides excepting Nb_2CuC as it has an additional transition metal Cu at A-site instead of A-group element that might be a barrier in understanding the general trend in typical Nb-based 211 MAX phases.

2. Method of calculations

The present calculations were performed using density functional theory (DFT) as implemented in the CASTEP code [38–40]. Exchange-correlation interactions were described with the generalized gradient approximation (GGA) corrected by Perdew, Burke and Ernzerhof (PBE) [41,42] scheme. The interaction between electrons and ion cores are treated with ultrasoft pseudopotential [43]. To expand the eigenfunctions of the valence electrons and the nearly free electrons, a plane wave basis set with cutoff energy of 550 eV is employed. To optimize the geometry via minimizing the total energy and internal forces BFGS minimization scheme is used because of its advantage of ability to perform cell optimization, including optimization at fixed external stress [44]. Brillouin zone integrations are performed with a Γ-centered k-point mesh of 10×10×2 grid in the Monkhorst-Pack (MP) scheme [45]. All the crystal structures are relaxed until the residual forces on the atoms have declined to less than 0.01 eV/Å, maximum stress less than 0.02 GPa, maximum displacement less than 5×10^{-4}Å, and energy per atom less than 5×10^{-6} eV.

The CASTEP code is embodied with the finite-strain theory to calculate the elastic properties of materials [46]. In this theory, a specified set of identical strains (deformations) is applied to the conventional unit cell, allowing the relaxation of the atomic degrees of freedom. Then resultant external stresses are calculated. The stress tensor has six stress components σ_{ij} for each strain δ_j applied to the conventional unit cell. Then elastic constants C_{ij} are calculated by solving a set of linear equations, $\sigma_{ij} = C_{ij}\delta_j$. This method is employed in the present study and it has already successfully predicted the elastic properties of a wide range of crystals [47–60].

To better understand the possible mechanisms of radiation tolerance in the Nb-based 211 MAX carbides, intrinsic defects (vacancies, antisite defects and interstitials) calculations are performed with DFT to determine the energetically favourable defect processes in Nb_2AC (A = Al, Ga, Ge, In, Sn, As, P, and S). Vacancies and antisites are assumed as isolated defects on each symmetrically distinct lattice site. All possible interstitial sites are considered for each element within the 211 MAX phase structure. A 3×3×1 supercell of 72 lattice sites (36 Nb, 18A, and 18 C) are used for defects calculations with a cutoff energy of 450 eV and k-point mesh of 3×3×2 grid in the MP scheme. These calculations were performed under constant pressure conditions.

3. Results and discussions

3.1. Optimized structure

The optimized structure of Nb_2AlC as a structural model of 211 MAX phases is shown in Fig. 1, indicating that MX slab is separated by one A-atomic layer. The calculated lattice parameters are listed in Table 1 along with reported measured values for comparison. Fig. 2 shows that the calculated lattice constants are consistent with the experimental ones. The lattice parameters of Nb_2SnC exhibit relatively large deviation of 1.27% for *a*. In the most cases, the GGA trend ($a_{calc,}$ $c_{calc.}$> $a_{expt,}$ $c_{expt.}$) is established. Violation is observed for the Ge-based phase, which is also observed for *c* in a previous study of Nb_2GeC [61]. It is worth mentioning that Nb_2GeC is synthesized only in the thin film form and during its fabrication some NbC_x phases are obtained. The phase impurity me be the possible reason of violation of GGA trend for Nb_2GeC. When the A-element moves from left to right across the periodic table in a period the lattice constant *a* increases, whereas the lattice constant *c* decreases followed by an increase for S.

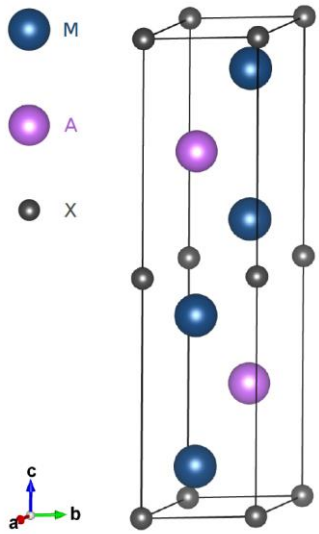

Fig. 1. The optimized structure of Nb_2AlC as a structural model of 211 MAX phases.

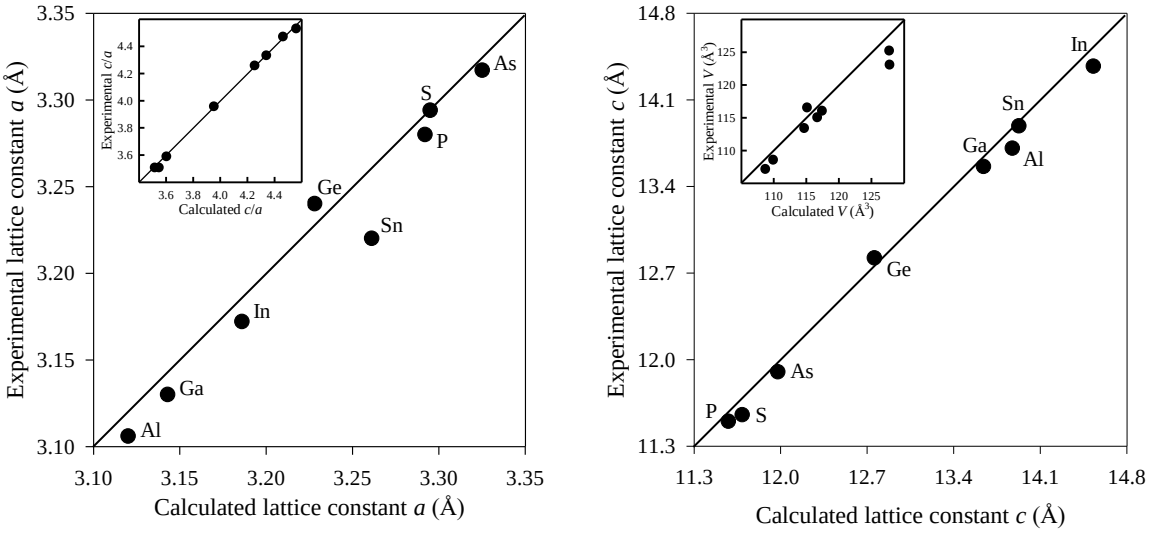

Fig. 2. Calculated versus experimental cell constants of Nb_2AC MAX phases.

Table 1. Calculated and experimental lattice constants of Nb-based 211 MAX carbides.

Phase	a (Å)	c (Å)	c/a	V (Å^3)	Remarks
Nb_2GaC	3.143	13.640	4.340	116.66	This calc.
	3.13	13.56	4.332	115.05	Expt. [1]
Nb_2PC	3.292	11.578	3.517	108.68	This calc.
	3.28	11.5	3.506	107.15	Expt. [1]
Nb_2AlC	3.120	13.926	4.463	117.41	This calc.
	3.106	13.888	4.471	116.03	Expt. [20]
Nb_2GeC	3.228	12.759	3.953	115.10	This calc.
	3.24	12.82	3.957	116.45	Expt. [61]
Nb_2SC	3.295	11.690	3.548	109.90	This calc.
	3.294	11.553	3.507	108.56	Expt. [62]
Nb_2AsC	3.325	11.977	3.602	114.67	This calc.
	3.317	11.90	3.588	113.39	Expt. [63]
Nb_2InC	3.186	14.528	4.560	127.72	This calc.
	3.172	14.37	4.530	125.21	Expt. [64]
Nb_2SnC	3.261	13.874	4.254	127.77	This calc.
	3.220	13.707	4.257	123.08	Expt. [65]

3.2. Elastic behaviour

Both elastic constants and moduli describe the elastic (i.e., mechanical) behaviour of materials. MAX phases have six different elastic constants C_{11}, C_{33}, C_{44}, C_{66}, C_{12}, and C_{13} as they crystallize in hexagonal space group $P6_3/mmc$. All elastic constants are independent excepting C_{66} since $C_{66} = (C_{11} - C_{12})/2$. Elastic constants ensure the mechanical stability of hexagonal crystals obeying the following conditions [66]:

$$C_{11} > 0,\ C_{33} > 0,\ C_{44} > 0,\ (C_{11} + C_{12})C_{33} > 2(C_{13})^2, \text{ and } (C_{11} - C_{12}) > 0 \quad (1)$$

The calculated elastic constants are listed in Table 2. These values are consistent with the ones reported in previous studies [19,27,29–37]. The present values meet the above conditions to be stable mechanically for the compounds studied here. The elastic constant C_{11} measures the elastic stiffness of the materials regarding (100)⟨100⟩ strain. In this view, Nb_2PC is the stiffest and Nb_2SnC is the softest material in this group. Regarding (001)⟨001⟩ strain, the elastic constant C_{33} also predict the same results, that is, Nb_2PC is the stiffest and Nb_2SnC is the softest one. The elastic constant C_{12} measures the resistance against deformation in the (110) plane along ⟨100⟩ direction. Therefore, Nb_2GeC is most rigid and Nb_2GaC is easily deformable materials among the compounds studied here. The low value of C_{12} and C_{13} imply that Nb_2GaC, Nb_2InC, Nb_2AlC, and Nb_2SnC are easier to shear along the b- and c-axis compared to other MAX phases under investigation when a stress is applied along the a-axis.

Elastic anisotropy is an inherent characteristic of solids. Primarily, it can be ensured from the elastic constants C_{11} and C_{33}. Either $C_{11} > C_{33}$ or $C_{33} > C_{11}$ is the indication of elastic anisotropy of crystals. For hexagonal crystals like MAX phases, a common anisotropy factor is $A = 4C_{44}/(C_{11}+C_{33}–2C_{12})$, which is calculated to give insight on the elastic shear anisotropy of Nb-based 211 MAX carbides and are listed in Table 2. Elastically, anisotropic crystals have A-value either greater or less than unity. Deviation from unity ΔA quantifies the degree of elastic anisotropy, which is shown in Fig. 3. Thus, Nb_2GeC is elastically highly anisotropic and Nb_2InC possesses low level of elastic anisotropy. Additionally A-value provides information regarding screw dislocation and cross-slip pining process in crystals. The larger A-value leads to the driving force (tangential force) acting on screw dislocations to stimulate the cross-slip pinning process [67]. The comparatively high A-value is inclined to elastically enhance the cross-slip pinning process in Nb_2GeC that is considerably reduced in Nb_2InC.

There is another anisotropy factor for hexagonal crystals that can be named compressibility anisotropy factor and is expressed as $k_c/k_a = (C_{11}+C_{12}–2C_{13})/(C_{33}–C_{13})$. This describes linear compressibility of c-axis relative to the a-axis. The calculated value listed in Table 2 for compounds

studied here implies that the Nb_2AlC is more compressible along c-axis than a-axis. For other phases, the compressibility is more profound along a-axis than c-axis, with most for Nb_2PC. Therefore, the anisotropy in compression of Nb_2AlC and Nb_2PC is large along c- and a-axis, respectively. $\Delta(k_c/k_a)$ defines the anisotropic level of the phases given in Fig. 3, which also exhibits the trend of elastic anisotropy level in Nb_2AC MAX phases with the A-elements. The trends of ΔA and A^U (A^U is discussed latter) are almost similar. $\Delta(k_c/k_a)$ shows an increasing trend from Al to P when one goes through one group elements to the next group elements and then shows a decreasing trend.

Table 2. Elastic constants C_{ij} (in GPa) and anisotropy factors A and k_c/k_a for Nb-based 211 MAX carbides.

Phase	C_{11}	C_{33}	C_{44}	C_{66}	C_{12}	C_{13}	A	k_c/k_a
Nb_2AlC	332.88	283.66	138.41	124.43	84.02	117.30	1.45	1.10
Nb_2GaC	322.88	280.85	126.36	122.73	77.42	129.54	1.47	0.93
Nb_2InC	280.36	266.05	103.67	100.35	79.63	112.73	1.29	0.88
Nb_2GeC	283.60	275.05	151.66	73.58	136.44	160.77	2.56	0.86
Nb_2SnC	263.65	260.44	109.52	87.53	88.59	121.38	1.56	0.79
Nb_2PC	372.81	406.77	193.48	129.40	114.01	172.21	1.78	0.61
Nb_2AsC	343.01	342.72	173.02	120.69	101.62	166.76	1.95	0.63
Nb_2SC	323.69	333.35	125.69	103.84	116.01	145.76	1.38	0.79

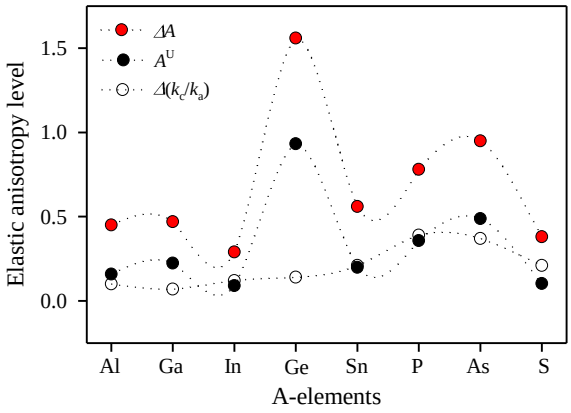

Fig. 3. Elastic anisotropic level in Nb_2AC MAX phases.

Elastic constants C_{ij} can be used to calculate the bulk modulus B and shear modulus G. According to Voigt, Reuss, and Hill (VRH) approximations [68–70] they are identified by using V, R, and H as subscripts to B and G and their calculated values are listed in Table 3. It is evident that Nb_2PC and Nb_2InC respectively, have highest and lowest value of B, indicating that they are respectively, most incompressible and compressible under pressure. They are also strongest and weakest materials in view of chemical bonding. The strength of chemical bonding should follow the order: Nb_2PC > Nb_2AsC > Nb_2SC > Nb_2GeC > Nb_2GaC > Nb_2AlC > Nb_2SnC > Nb_2InC. For comparison, we have experimental value of B 165 and 208 GPa for Nb_2AlC [71,72], 180±5 GPa for Nb_2SnC [73], 224±2 GPa for Nb_2AsC [74]. These values are consistent with the present values. Shear modulus for the compounds studied here is smaller in magnitude than the respective bulk modulus, indicating that the mechanical stability of these solids is controlled by shear modulus. Nb_2PC and Nb_2SnC respectively, have highest and lowest value of G, indicating that the shape change is easier in Nb_2SnC and not in Nb_2PC compared with other Nb_2AC phases. Shear modulus is highly correlated with the materials' hardness. Accordingly, Nb_2PC and Nb_2SnC respectively, are the hardest and softest materials among Nb-based 211 MAX phase carbides. The hardness should follow the rank: Nb_2PC > Nb_2AsC > Nb_2AlC > Nb_2GaC > Nb_2SC > Nb_2InC > Nb_2GeC > Nb_2SnC.

Bulk to shear modulus ratio B_H/G_H known as Pugh's ratio plays a vital role to characterize an important mechanical phenomena in materials [75]. To judge the mechanical failure mode of solids, Pugh's ratio with a threshold value of 1.75 serves as an indicator. Brittle failure occurs for a material whose Pugh's ratio is less than 1.75 and ductile failure happens for a material having a value greater than 1.75. Accordingly, Nb_2GeC, Nb_2SnC, and Nb_2SC are ductile materials and the remaining majorities are brittle materials. Indeed, most of the MAX phases are brittle in nature [3,32,49–56]. Nb_2GeC is highly ductile and Nb_2AlC is more brittle in this group. In ductile materials, cracks progress sluggishly when plastic deformation occurs, while in brittle materials, cracks extend rapidly when stress is applied.

Young's modulus for polycrystalline aggregates are calculated from B and G, $E = 9BG/(3B+G)$ and listed in Table 4. E is a measure of the ability of a material to resist changes in length when under lengthwise tension or compression. It is evident that Nb_2PC and Nb_2SnC, respectively have highest and lowest value of E, signifying that they are respectively, most stiff and flexible, under tension or compression compared with other Nb_2AC phases. Young's modulus is also a measure of materials' hardness [19]. Based on E, if we rank the compounds studied here for hardness, we have the same order based on G, excepting an interchange of positions between Nb_2InC and Nb_2GeC. Young's modulus also has a good relation with the critical thermal shock resistance, $R \propto 1/E$ [55], implying that the lower the E better the R. Thus Nb_2SnC has better thermal shock resistance among all the Nb-based 211 MAX phase carbides studied here. Better thermal shock resistance is a precondition for a solid to be used as a thermal barrier coating (TBC) material. Fig. 4 shows a comparative picture of elastic moduli to understand at a glance.

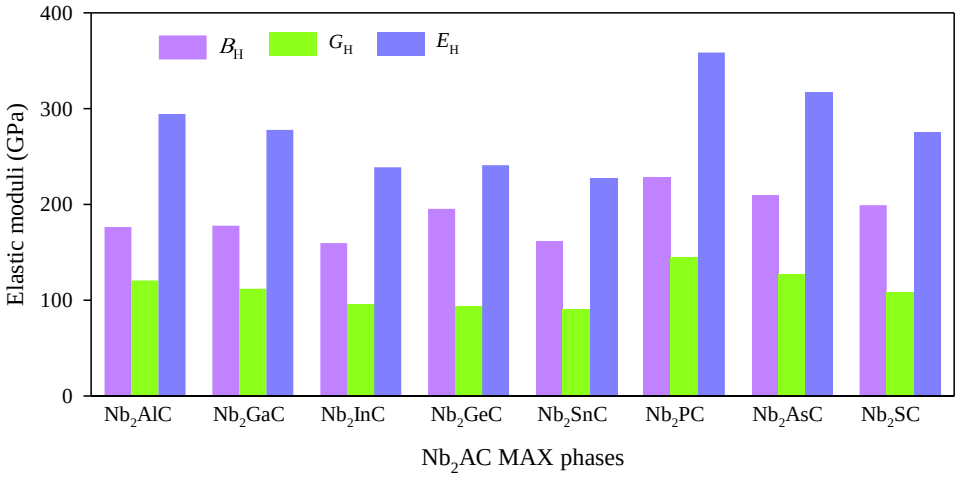

Fig. 4. Elastic moduli of Nb_2AC MAX phases.

Poisson's ratio for polycrystalline aggregates are calculated from B and G, $\sigma = (3B–2G)/(6B+2G)$, and are listed in Table 4 and shown in Fig. 5 along with B_H/G_H. Poisson's ratio is a decisive factor for many characterizing issues in solids. Poisson's ratio also justifies the failure modes of solids with a critical value of 0.26 [3]. Ductile and brittle materials have respectively, larger and smaller values than 0.26. This factor also finds the ductile/brittle materials as Pugh's ratio does. In this scale, Nb_2GeC is again highly ductile and Nb_2AlC is the most brittle in the groups. The A-group elements Al, Ga, and In come from group 13. The 211 MAX carbides with these elements show a decreasing trend of brittleness when we moves from up to down according to both Pugh's and Poisson's ratios. The In-based Nb_2InC reaches near the brittle-ductile borderline. Ge is the first element of the next group 14 and the Ge-based Nb_2GeC crosses the borderline and become a highly ductile material. Sn is the second element of the same group 14 and Sn containing Nb_2SnC shows a decrease in its ductility and reaches near the brittle-ductile borderline. P is the first element of the group 15 and Nb_2PC crosses the borderline and become a brittle one. As is the second element of group 15 and Nb_2AsC show a decreasing trend of brittleness as of the element of group 13. S is the first element of the next group 16 and Nb_2SC crosses the borderline and become a ductile material. It exhibits the same trend of Nb_2GeC that contains the first element of group 14.

A crystalline solid is always stable under either central force or non-central force. A material will be stabilized by central force if its Poisson's ratio lies between 0.25 and 0.50, otherwise it will be stabilized by non-central force [3]. Accordingly, Nb_2InC, Nb_2GeC, Nb_2SnC, and Nb_2SC are stabilized with central force and the remaining phases with non-central force. It is observed that the ductile materials are mainly central force solids; while the brittle materials are non-central force ones. Poisson's ratio can predict atomic bonding nature in crystals by identifying the purely covalent crystals with a value of 0.10 and totally metallic crystals with a value of 0.33 [19]. It is expected that all the Nb-based 211 MAX carbides are characterized by partially metallic and covalent bonding as their Poisson's ratio lies between 0.10 and 0.33. However, the brittle phases are more covalent than the ductile ones. For comparison, we have experimental value of 0.21 for Nb_2AlC [71], which is almost similar to the present value of 0.222.

Table 3. Bulk and shear moduli (in GPa) and Pugh's ratio of Nb-based 211 MAX carbides.

Phase	B_V	B_R	B_H	G_V	G_R	G_H	B_H/G_H
Nb_2AlC	176.29	176.18	176.24	122.30	118.54	120.42	1.46
Nb_2GaC	177.74	177.69	177.71	114.43	109.54	111.98	1.59
Nb_2InC	159.65	159.48	159.57	96.31	94.63	95.47	1.67
Nb_2GeC	195.36	195.19	195.27	101.00	85.14	93.07	2.10
Nb_2SnC	161.16	160.65	160.91	91.74	88.28	90.01	1.79
Nb_2PC	229.92	226.83	228.37	149.54	139.91	144.72	1.58
Nb_2AsC	211.00	208.98	209.99	132.92	121.32	127.12	1.65
Nb_2SC	199.53	198.87	199.20	109.26	107.13	108.19	1.84

Table 4. Young's modulus (in GPa), Poisson's ratio and universal anisotropy index of Nb-based 211 MAX carbides.

Phase	E_V	E_R	E_H	σ_V	σ_R	σ_H	A^U
Nb_2AlC	298.00	290.47	294.25	0.218	0.225	0.222	0.159
Nb_2GaC	282.63	272.59	277.63	0.235	0.244	0.240	0.224
Nb_2InC	240.57	237.01	238.79	0.249	0.252	0.251	0.090
Nb_2GeC	258.45	222.99	240.93	0.280	0.310	0.294	0.932
Nb_2SnC	231.33	223.84	227.59	0.261	0.268	0.264	0.199
Nb_2PC	368.68	348.15	358.45	0.233	0.244	0.238	0.358
Nb_2AsC	329.56	304.95	317.33	0.240	0.257	0.248	0.488
Nb_2SC	277.18	272.46	274.82	0.268	0.272	0.270	0.103

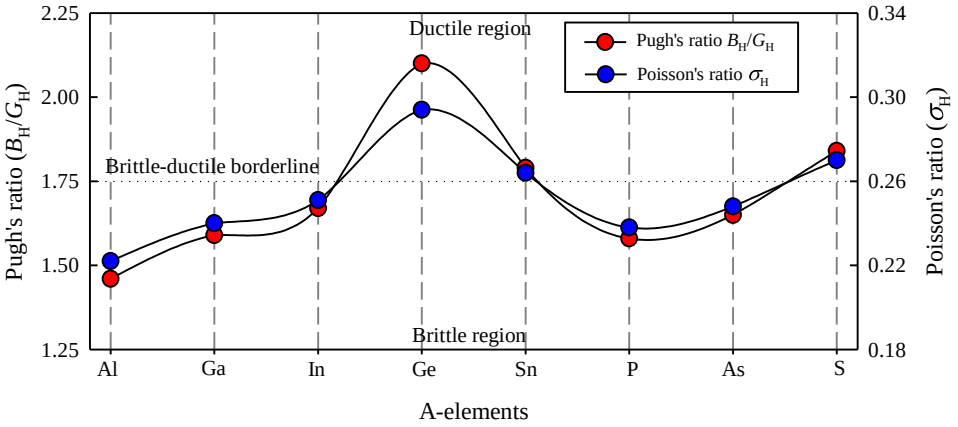

Fig. 5. Pugh's and Poisson's ratio of Nb_2AC MAX phases.

Depending on Voigt and Reuss limit of bulk and shear moduli, an anisotropy factor is defined as $A^U = 5(G_V/G_R) + (B_V/B_R) - 6$, which is known as universal anisotropy index as it is applicable for all kind of crystals [76] with different symmetries. The calculated value of A^U is listed in Table 4 and shown in Fig.

3, indicating that anisotropy level is high in Nb_2GeC and low in Nb_2InC. This prediction is same as predicted from shear anisotropy factor *A*. A^U directly measures the anisotropy level in crystals.

3.3 Defect processes

The reason for examining the point defect processes of materials is that they can determine their macroscopic properties for example their radiation tolerance. As it has been discussed in previous work this is particularly important as MAX phases are considered for nuclear applications [77,78]. From a physical viewpoint, the ability of a material to resist radiation will be dependent upon the ability of the material to form and accommodate point defects. In that respect, a high concentration of defects can result to the destabilization of the material [79-81].

To calculate the defect processes (refer to Table 5) we have considered all possible point defects and importantly all the possible interstitial defects (The lowest energy interstitial sites for the Nb_2AC MAX phases are given in Table 6). In Table 5, we present all the defect processes considered here and the corresponding defect energies in Kröger–Vink notation [82]. In this notation, Nb_i will denote a Nb interstitial defect, Nb_A an antisite defect (i.e. a Nb atom in an A-site) and V_{Nb} a vacant Nb site.

Table 5. The defect process reaction (Frenkel 1-3; antisite 4-6) energies for the Nb_2AC MAX phase.

Defect Reactions	Defect energy (eV)							
	Nb_2AlC	Nb_2AsC	Nb_2GaC	Nb_2GeC	Nb_2InC	Nb_2PC	Nb_2SC	Nb_2SnC
(1) $Nb_{Nb} \rightarrow V_{Nb} + Nb_i$	7.8909	8.4693	5.4662	5.9219	7.7613	9.2965	6.1069	8.1782
(2) $A_A \rightarrow V_A + A_i$	4.5934	7.7893	3.7765	4.5134	6.6649	7.5774	7.3398	8.3452
(3) $C_C \rightarrow V_C + C_i$	3.0938	4.4458	3.9199	3.1356	4.9546	4.2133	3.7014	4.8415
(4) $Nb_{Nb} + A_A \rightarrow Nb_A + A_{Nb}$	2.9800	8.3839	4.2095	5.8330	3.5978	10.0846	9.7703	5.1802
(5) $Nb_{Nb} + C_C \rightarrow Nb_C + C_{Nb}$	15.8236	12.4426	15.2602	13.5318	13.9492	13.0953	10.2005	13.4818
(6) $A_A + C_C \rightarrow A_C + C_A$	9.5503	4.0405	8.3706	5.5303	12.0852	2.8984	2.7874	10.1008
(7) $Nb_i + V_A \rightarrow Nb_A$	-5.7821	-3.7175	-3.4084	-2.9738	-6.1817	-2.2933	-0.5443	-6.4284
(8) $C_i + V_A \rightarrow C_A$	0.8008	-2.6554	-0.0104	-0.3059	0.6196	-3.2429	-3.1738	0.1920
(9) $Nb_i + A_A \rightarrow Nb_A + A_i$	-1.1887	4.0718	0.3681	1.5396	0.4831	5.2841	6.7956	1.9167
(10) $A_i + V_{Nb} \rightarrow A_{Nb}$	-3.7222	-4.1572	-1.6248	-1.6284	-4.6466	-4.4961	-3.1321	-4.9147
(11) $C_i + V_{Nb} \rightarrow C_{Nb}$	1.8521	-0.4272	1.0050	1.3226	0.1184	-1.0242	-0.3285	0.9071
(12) $Nb_i + V_C \rightarrow Nb_C$	2.9868	-0.0453	4.8691	3.1518	1.1148	0.6096	0.7208	-0.4449
(13) $A_i + V_C \rightarrow A_C$	1.0624	-5.5393	0.6846	-1.8128	-0.1539	-5.6494	-5.0800	-3.2778
(14) $Nb_i + C_C \rightarrow Nb_C + C_i$	6.0806	4.4005	8.7890	6.2874	6.0695	4.8229	4.4221	4.3965
(15) $A_i + Nb_{Nb} \rightarrow A_{Nb} + Nb_i$	4.1687	4.3122	3.8414	4.2934	3.1147	4.8005	2.9748	3.2635
(16) $A_i + C_C \rightarrow A_C + C_i$	4.1562	-1.0934	4.6045	1.3228	4.8008	-1.4361	-1.3787	1.5637
(17) $C_i + Nb_{Nb} \rightarrow C_{Nb} + Nb_i$	9.7430	8.0421	6.4712	7.2445	7.8797	8.2724	5.7784	9.0853
(18) $C_i + A_A \rightarrow C_A + A_i$	5.3941	5.1339	3.7661	4.2075	7.2844	4.3345	4.1660	8.5371

The most important defect processes indicating radiation tolerance are the Frenkel reactions (Table 5, relations 1-3) and the antisite reactions (Table 5, relations 4-6). Considering the materials with higher Frenkel and antisite energies will be more radiation persistent and in that respect Nb_2SnC is the better material as it has higher defect energies than the other Nb-MAX phases considered (Table 5, relations 1-6). Relations 7-12 (refer to Table 5) reveal whether interstitial defects and vacancies are energetically

favourable to recombine and effectively to form antisite defects or if they rather remain as isolated defects. Finally, relations 13-18 (refer to Table 5) examine whether in a radiation environment where there is an over stoichiometry of self-interstitials there is the possibility to form antisite defects.

Table 6. The lowest energy interstitial sites for the Nb_2AC MAX phases.

Phase	Atom	Energetically preferable interstitials sites		
Nb_2AlC	Nb	0.0007	0.9993	0.7226
	Al	0.9979	0.0021	0.7509
	C	0.3335	0.6665	0.7500
Nb_2AsC	Nb	0.9961	0.9984	0.7065
	As	0.9942	0.9974	0.7490
	C	0.3330	0.6646	0.7497
Nb_2GaC	Nb	0.9015	0.2232	0.7511
	Ga	0.3829	0.2662	0.7497
	C	0.3331	0.6642	0.7499
Nb_2GeC	Nb	0.3312	0.2400	0.7497
	Ge	0.9986	0.0010	0.7494
	C	0.3330	0.6648	0.7498
Nb_2InC	Nb	0.3198	0.2298	0.7498
	In	0.3360	0.2453	0.7498
	C	0.9984	0.0012	0.6550
Nb_2PC	Nb	0.9995	0.9998	0.7177
	P	0.9999	0.9998	0.7490
	C	0.3329	0.6644	0.7497
Nb_2SC	Nb	0.0001	0.0014	0.7513
	S	0.3269	0.2822	0.7503
	C	0.8618	0.9313	0.9472
Nb_2SnC	Nb	0.3226	0.2176	0.7498
	Sn	0.3809	0.2889	0.7495
	C	0.3326	0.6638	0.7497

4. Conclusions

In the present study, DFT calculations were employed to investigate the elastic properties and defect processes of Nb-based 211 MAX phases. The lattice constant *a* exhibits the tendency to increase when the *A*-group element moves from left to right through the periodic table within a period and the lattice constant *c* decreases followed by an increase for S. All the compounds studied here are mechanically stable and elastically anisotropic. Nb_2GeC is expected to be elastically high and Nb_2InC to be low anisotropic. The cross-slip pinning process is enhanced in Nb_2GeC and is significantly reduced in Nb_2InC. Among the Nb-based 211 MAX phases, Nb_2GeC, Nb_2SnC, and Nb_2SC are expected to be ductile i.e., damage tolerant and the rest to be brittle. Nb_2GeC is predicted to be highly ductile and Nb_2AlC to be more brittle. Nb_2PC is expected to be stiffer, while Nb_2SnC to be more flexible under tension or compression. Nb_2SnC has the best thermal shock resistance among the Nb-based 211 MAX phase carbides studied here. Finally, it is anticipated that Nb_2SnC has also the highest radiation resistance.

CRediT authorship contribution statement

M.A. Hadi: Conceptualization, Investigation, Data curation, Methodology, Formal analysis, Writing - original draft. **S.-R.G. Christopoulos:** Investigation, Data curation, Methodology. **A. Chroneos**: Formal analysis, Writing, Review & editing. **S.H. Naqib**: Formal analysis, Review & editing. **A.K.M.A. Islam**: Formal analysis, Review & editing.

Declaration: There is no conflict of interest to declare.

Reference

[1] M.W. Barsoum, Prog. Solid State Chem. **28** (2000) 201–281.
[2] T. Rackl, L. Eisenburger, R. Niklaus, and D. Johrendt, Phys. Rev. Mater. **3**, (2019) 054001.
[3] M.A. Hadi, Computational Materials Science **117** (2016) 422–427.
[4] M.W. Barsoum, MAX Phases, Wiley-VCH Verlag GmbH & Co. KGaA, Weinheim, Germany, 2013,
[5] M.W. Barsoum, M. Radovic, Annu. Rev. Mater. Res. 41 (2011) 195–227.
[6] D.J. Tallman, L. He, B.L. Garcia-Diaz, E.N. Hoffman, G. Kohse, R.L. Sindelar, et al., J. Nuclear Mater. 468 (2016) 194–206.
[7] D.J. Tallman, L. He, J. Gan, E.N. Caspi, E.N. Hoffman, M.W. Barsoum, J. Nuclear Mater. 484 (2017) 120–134.
[8] C. Ang, C. Silva, C. Shih, T. Koyanagi, Y. Katoh, S.J. Zinkle, Scr. Mater 114 (2016) 74–78.
[9] E.N. Hoffman, D.W. Vinson, R.L. Sindelar, D.J. Tallman, G. Kohse, M.W. Barsoum, Nuclear Eng. Des. 244 (2012) 17–24.
[10] W.E. Lee, M. Gilbert, S.T. Murphy, R.W. Grimes, J. Am. Ceram. Soc. 96 (2013) 2005–2030.
[11] E. Zapata-Solvas, S.-R.G. Christopoulos , N. Ni, D.C. Parfitt, D. Horlait, M.E. Fitzpatrick , A. Chroneos, and W. E. Lee, J. Am. Ceram. Soc. **100** (2017) 1377-1387.
[12] T. Lapauw, K. Lambrinou, T. Cabioc'h, J. Halim, J. Lu, A. Pesach, et al., J. Eur. Ceram Soc. 36 (2016) 1847–1853.
[13] T. Lapauw, J. Halim, J. Lu, T. Cabioc'h, L. Hultman, M.W. Barsoum, et al., J. Eur. Ceram Soc. 36 (2015) 1–5.
[14] T. Lapauw, D. Tytko, K. Vanmeensel, S. Huang, P.-P.Choi, D. Raabe, et al., Inorg. Chem. 55 (2016) 5445–5452.
[15] E. Zapata-Solvas, S.-R.G. Christopoulos, N. Ni, D.C. Parfitt, D. Horlait, M.E. Fitz- patrick, et al., J. Am. Ceram. Soc. 2 (2017) 27–11.
[16] E. Zapata-Solvas, M.A. Hadi, D. Horlait, D.C. Parfitt, A. Thibaud, A. Chroneos, et al., J. Am. Ceramic Soc. 100 (2017) 3393-3401.
[17] D. Bowden, J. Ward, S. Middleburgh, S. de Moraes Shubeita, E. Zapata-Solvas, T. Lapauw, J. Vleugels, K. Lambrinou, W.E. Lee, M. Preuss, and P. Frankel, Acta Materialia 183, 24-45 (2020)
[18] T. Deng, J. Sun, P. Tai, and Y. Wang et al., Acta Materialia 189, 188-203 (2020)
[19] M.A. Hadi, J. Phys. Chem. Solids **138** (2020) 109275.
[20] I. Salama, T. El-Raghy, M.W. Barsoum, J. Alloys Compd. 347 (2002) 271–278.
[21] W. Zhang, N. Travitzky, C.F. Hu, Y.C. Zhou, P. Greil, J. Am. Ceram. Soc. 92 (2009) 2396–2399.
[22] C.L. Yeh, C.W. Kuo, J. Alloys Compd. 496 (2010) 566–571.
[23] M.F. Cover, O. Warschkow, M.M.M. Bilek and D.R. McKenzie, J. Phys. Condens. Matter 21 (2009) 305403.
[24] M. Khazaei, A. Ranjbar, K. Esfarjani, D. Bogdanovski, R. Dronskowski and S. Yunoki, Phys. Chem. Chem. Phys. 20 (2018) 8579-8592.
[25] P. Simon, Y. Gogotsi, and B. Dunn, Science343 (2014)6176.
[26] S. Zhao, Y. Dall'Agnese, X. Chu, X. Zhao, Y. Gogotsi, and Y. Gao, ACS Energy Lett. 4 (2019) 2452−2457.
[27] M.T. Nasir, A.K.M.A. Islam, Comp. Mater. Sci. 65 (2012) 365–371.
[28] H. Dinga, Y. Li, J. Lu, K. Luo, K. Chen, M. Li, P.O.A. Persson, L. Hultman, P. Eklund, S. Du, Z. Huang, Z. Chai, H. Wang, P. Huang, Q. Huang, Mater. Res. Lett. **7** (2019) 510-516.
[29] M.B. Kanoun, S. Goumri-Said, and A.H. Reshak, Comp. Mater. Sci. 47 (2009) 491–500.
[30] H. Wang, Y. Zhan, and M. Pang, Comp. Mater. Sci. 54 (2012) 16–22.
[31] A. Bouhemadou and R. Khenata, J. Appl. Phys. 102 (2007) 043528.
[32] M.A. Hadi, N. Kelaidis, S.H. Naqib, A. Chroneos, and A.K.M.A. Islam, J. Phys. Chem. Solids 129 (2019) 162-171.
[33] A. Bouhemadou, Appl. Phys. A 96 (2009) 959–967.

[34] W.-Y. Ching, Y. Mo, S. Aryal, and P. Rulis, J. Am. Ceram. Soc. 96 (2013) 2292-2297.
[35] J. Wang and Y. Zhou, Phys. Rev. B 69 (2004) 214111.
[36] I.R. Shein, A.L. Ivanovskii, Physica B 410 (2013) 42–48.
[37] Z. Sun, S. Li, R. Ahuja, J.M. Schneider, Solid State Commun. 129 (2004) 589–592.
[38] P. Hohenberg and W. Kohn, Phys. Rev. **136** (1964) B864.
[39] W. Kohn and L.J. Sham, Phys. Rev. **140** (1965) A1133.
[40] S. J. Clark, M. D. Segall, C. J. Pickard, P. J. Hasnip, M. I. J. Probert, K. Refson, and M. C. Payne, Z. Kristallogr. **220** (2005) 567.
[41] J.P. Perdew, J.A. Chevary, S.H. Vosko, K.A. Jackson, M.R. Pederson, D.J. Singh, and C. Fiolhais, Phys. Rev. B **48** (1993) 4978.
[42] J. P. Perdew, K. Burke, M. Ernzerhof, Phys. Rev. Lett. **77** (1996) 3865-3868.
[43] D. Vanderbilt, Phys. Rev. B **41** (1990) 7892.
[44] T.H. Fischer and J. Almlof, J. Phys. Chem. **96** (1992) 9768.
[45] H. J. Monkhorst and J. D. Pack, Phys. Rev. B **13** (1976) 5188.
[46] F. D. Murnaghan, Finite Deformation of an Elastic Solid (Wiley, New York, 1951).
[47] M. Mozahar Ali, M.A. Hadi, M.L. Rahman, F.H. Haque, A.F.M.Y. Haide, M. Aftabuzzaman, J. Alloys and Compounds 821 (2020) 153547.
[48] M. N. Islam, M. A. Hadi, and J. Podder, AIP Advances 9 (2019) 125321.
[49] P.P. Filippatos, M.A. Hadi, S.-R.G. Christopoulos, A. Kordatos, N. Kelaidis, M.E. Fitzpatrick, M. Vasilopoulou and A. Chroneos, Materials 12 (2019) 4098.
[50] M.A. Hadi, M.A. Rayhan, S.H. Naqib, A. Chroneos, A.K.M.A. Islam, Computational Materials Science 170 (2019) 109144.
[51] M.A. Hadi, U. Monira, A. Chroneos, S.H. Naqib, A.K.M.A. Islam, N. Kelaidis, R.V. Vovk Journal of Physics and Chemistry of Solids 132 (2019) 38–47.
[52] M. Roknuzzaman, M.A. Hadi, M. A. Ali, M.M. Hossain, N, Jahan, M.M. Uddin, J.A. Alarco, K. Ostrikov, J. Alloys Comp. 727 (2017) 616-626.
[53] M.A. Hadi, S.-R.G. Christopoulos, S.H. Naqib, A. Chroneos, M.E. Fitzpatrick, A.K.M.A. Islam, Journal of Alloys and Compounds 748 (2018) 804-813.
[54] S.-R. G. Christopoulos, P. P. Filippatos, M. A. Hadi, N. Kelaidis, M. E. Fitzpatrick, A. Chroneos, Journal of Applied Physics 123 (2018) 025103.
[55] M. Roknuzzaman, M.A. Hadi, M.J. Abedin, M.T. Nasir, A.K.M.A. Islam, M.S. Ali, K. Ostrikov, Comp. Mater. Sci. 113 (2016) 148-153.
[56] M.A. Hadi, M. Roknuzzaman, A. Chroneos, S.H. Naqib, A.K.M.A. Islam, R.V. Vovk, K. Ostrikov, Computational Materials Science 137 (2017) 318–326.
[57] M. A. Hadi, M. N. Islam, M. H. Babu, Z. Naturforsch. A 74 (2019) 71.
[58] A.M.M. Tanveer Karim, M.A. Hadi, M.A. Alam, F. Parvin, S.H. Naqib, A.K.M.A. Islam, Journal of Physics and Chemistry of Solids 117 (2018) 139–147.
[59] M. T. Nasir, M. A. Hadi, M. A. Rayhan, M. A. Ali, M. M. Hossain, M. Roknuzzaman, S. H. Naqib, A. K. M. A. Islam, M. M. Uddin, and K. Ostrikov, Physica Status Solidi B 254 (2017) 1700336.
[60] M. A. Ali, M. A. Hadi, M. M. Hossain, S. H. Naqib, A. K. M. A. Islam, Physica. Status Solidi B 254 (2017) 1700010.
[61] P. Eklund, M. Dahlqvist, O. Tengstrand, L. Hultman, J. Lu, N. Nedfors, U. Jansson, J. Rose, Phys. Rev. Lett. 109 (2012) 035502.
[62] K. Sakamaki, H. Wada, H. Nozaki, Y. Onuki, M. Kawai, Solid State Commun. 112 (1999) 323.
[63] D. Music, Z. Sun and J. M. Schneider, Phys. Rev. B71 (2005) 092102.
[64] A.D. Bortolozo, Z. Fisk, O.H. Sant'Anna, C.A.M. dos Santos, A.J.S. Machado, Physica C 469 (2009) 256.
[65] A.D. Bortolozo, O.H. Sant'Anna, M.S. da Luz, C.A.M. dos Santos, A.S. Pereira, K.S. Trentin, A.J.S. Machado, Solid State Commun. 139 (2006) 57.
[66] M. Born, On the stability of crystal lattices. I, Mathematical Proceedings of the Cambridge Philosophical Society, Cambridge University Press, 1940, pp. 160.

[67] M.H. Yoo, Scr. Metall. 20 (1986) 915–920.
[68] W. Voigt, LehrbuchderKristallphysik, Teubner, Leipzigund Berlin. l928.
[69] A. Reuss, Z. Angew. Math.Mech. **9** (1929) 49.
[70] R. Hilk, Proc. Phvs. Soc. A **65** (1952) 349.
[71] J.D. Hettinger, S.E. Lofland, P. Finkel, J. Palma, K. Harrell, et al. ,Phys. Rev. B72 (2005)115120.
[72] B. Manoun, R.P. Gulve, S.K. Saxena, S. Gupta, M.W. Barsoum, C.S. Zha, Phys. Rev. B73 (2006) 024110.
[73] T. El-Raghy, S. Chakraborty, M.W. Barsoum, J. Eur. Ceram. Soc.20 (2000) 2619–25.
[74] R.S. Kumar, S. Rekhi, A.L. Cornelius, M.W. Barsoum, Appl. Phys. Lett.86 (2005) 111904.
[75] S.F. Pugh, Philos. Mag. 45 (1954) 823-843.
[76] I. Shivakumar, Ranganathan, M. Ostoja-Starzewski, Phys. Rev. Lett. 101 (2008) 055504.
[77] D. Horlait, S.C.Middleburgh, A. Chroneos, W.E. Lee, Sci. Rep. 6 (2016) 18829.
[78] D. Horlait, S. Grasso, A. Chroneos, W.E. Lee, Mater. Res. Lett. 4 (2016) 137-133.
[79] W.J. Weber, Radiation Effects and Defects in Solids **77**(1983) 295-308.
[80] F.W. ClinardJr, D.L. Rohr, R.B. Roof., Nucl. Instrum. Methods Phys. Res. B**1**, (1984) 581-586.
[81] K.E. Sickafus, L. Minervini, R.W. Grimes, J.A. Valdez, M. Ishimaru, F. Li, K.J. McClellan, T. Hartmann, Science 289 (2000) 748-751.
[82] F.A. Kröger, H.J. Vink, Solid State Phys.,3(1956) 307-435.